

Climate change exacerbated heavy rainfall leading to large scale flooding in highly vulnerable communities in West Africa

Mariam Zachariah¹, Clair Barnes¹, Caroline Wainwright¹, Richard Ayodeji Balogun², Derbetini A. Vondou³, Elijah Adesanya Adefisan², Eniola Olaniyan⁴, Kamoru Abiodun Lawal⁴, Audrey Brouillet⁵, Benjamin Sultan⁵, Sjoukje Philip⁶, Sarah Kew⁶, Robert Vautard⁷, Gerbrand Koren⁸, Piotr Wolski⁹, Maja Vahlberg¹⁰, Roop Singh¹⁰, Cheikh Kane^{10,12}, Maarten van Aalst^{10,11}, Lisa Thalheimer¹³, Sihan Li¹⁴, Friederike E. L. Otto¹

1. *Grantham Institute, Imperial College London, UK*
2. *Department of Meteorology and Climate Science, Federal University of Technology, Akure Nigeria.*
3. *Laboratory for Environmental Modelling and Atmospheric Physics, University of Yaounde I, Cameroon*
4. *Nigerian Meteorological Agency, Abuja*
5. *ESPACE-DEV, Univ Montpellier, IRD, Univ Guyane, Univ Reunion, Univ Antilles, Univ Avignon, Montpellier, France*
6. *Royal Netherlands Meteorological Institute (KNMI), De Bilt, The Netherlands*
7. *Institut Pierre-Simon Laplace, Paris, France*
8. *Copernicus Institute of Sustainable Development, Utrecht University, Utrecht, the Netherlands*
9. *Climate System Analysis Group, University of Cape Town, Cape Town, South Africa*
10. *Red Cross Red Crescent Climate Centre, The Hague, the Netherlands*
11. *University of Twente, The Netherlands*
12. *Institut de Recherche pour le Développement, U01000/99AA01, Marseille, France*
13. *United Nations University, Institute for Environment and Human Security, Bonn, Germany*
14. *Department of Geography, University of Sheffield*

Main findings

- The flooding occurred as a consequence of above average rainfall throughout the 2022 rainy season exacerbated by shorter spikes of very heavy rain leading to flash floods as well as riverine floods. We therefore consider seasonal average rainfall over Lake Chad and 7-day maximum rainfall along the lower Niger Basin as the basis for our analysis.
- The flooding was further driven by the release of the Lagdo Dam in Cameroon, which is part of a river management system that was designed to be accompanied by another dam in Nigeria that has not been completed.
- The devastating impacts were further exacerbated by the proximity of human settlements, infrastructure (homes, buildings, bridges), and agricultural land to flood plains, underlying vulnerabilities driven by high poverty rates and socioeconomic factors (e.g. gender, age, income, and education), and ongoing political and economic instability.
- We also analyse how climate change from human activities, which includes greenhouse gas emissions as well as changes in aerosol pollution and other gases affect the rainfall in the region.

- To do this we analyse whether and to what extent human-caused climate change altered the likelihood and intensity of the seasonal rain over the Lake Chad Basin, and the peak 7-day rainfall over the lower Niger Basin. We look at both the historical record of weather data, and climate models with and without human activities altering the climate.
- Many of the available state-of-the-art climate models struggle to simulate the rainfall characteristics. Those that pass our evaluation test generally also show an increase in likelihood and intensity of extreme rainfall, in particular over the Lake Chad Basin.
- For the 7-day maximum rainfall over the lower Niger Basin, models and observations give very similar results, so we conclude that climate change made the event about twice as likely and approximately 5% more intense.
- For the seasonal rainfall over the Lake Chad region, we conclude that climate change made the event about 80 times more likely and approximately 20% more intense.
- Observations show a larger increase than the models, but there are large uncertainties in these estimates due to the high variability in rainfall in the region, and observed changes can have a variety of drivers, including, but not limited to, climate change. The increase in rainfall shown by the models is largely significant, but smaller.
- As a result of events like these becoming more likely as the planet has warmed, both events are not very rare in today's climate, with a return time of about 1 in 10 years for the seasonal rain over the Lake Chad Basin and a 1 in 5 year event for the 7-day seasonal maximum over the lower Niger Basin.
- Looking at the future, for a climate 2°C warmer than in preindustrial times, models suggest that rainfall intensity will increase further, but not as strongly, suggesting that the strong trend observed in the last 30 years, in part, represents a change in the atmospheric dynamics e.g. through climate change-induced changes in ocean temperatures and a trend due to changes in aerosol pollution, in addition to greenhouse gases.
- Both current conditions and the potential further increase in extreme rainfall over both basins and the fact that the event was not unusual in the current climate highlight that there is an urgent need to drastically improve water management and reduce vulnerability to seasonal rainfall.

1 Introduction

Annually, during the peak to late monsoon season between June and September/early October, West African sub-region experience heavy downpours, resulting in floods in most parts of sub-Saharan Africa ([Adefisan, 2018](#); [Balogun et al. 2019](#); [Balogun et al. 2021](#); [Balogun et al. 2022](#); [UN Floods](#)). Africa is the second worst continent affected by floods, after Asia, based on extent, casualties, and frequencies ([Few, 2003](#); [Tschakert et al. 2010](#)). These heavy rainfalls are usually from deep westward propagating convective systems embedded within the monsoon systems ([Pante and Knippertz, 2019](#)), and the Intertropical Discontinuity migrating northward, thus allowing influx of moisture from the Atlantic Ocean. The West African rainy season runs between May and October, with local variations, including southern parts of the region which experience two peaks of rain within the season, separated by the Little Dry Season ([Dunning et al., 2016](#); [WFP, 2021](#); [Klein et al., 2021](#) and [Adefisan 2022](#)). In 2022, the rains arrived early and were well above normal in many regions ([Ramadane, 6 September 2022](#)), leading to both fluvial (or riverine) and pluvial (rainfall-related) flood events, from Senegal to Cameroon ([UNHCR, 2022](#)). The situation was anticipated by the Regional Climate Outlook Forum for West Africa, Chad and Cameroon which emitted an alert in early May on the risk of a longer and

more intense rainy season than normal ([Centre Régional AGRHYMET, 2022](#)). This alert was based on the El Niño Southern Oscillation (ENSO) forecast from early April indicating a continuation of La Niña during July-August-September 2022 which is associated with more rainfall in the Sahel ([Goldenberg and Shapiro 1996](#); [Sheen et al. 2017](#)).

The eastern parts of West Africa including the Lake Chad Basin, northern Cameroon, Chad, as well as the central (Burkina Faso, Cote d'Ivoire) and the north-western regions (coastal Senegal and western Mauritania) began witnessing wetter-than-normal conditions, from the beginning of the season ([Reliefweb, 27 September 2022](#)). The abundant rainfall season was also characterized by early onset, which led to the drainage systems being quickly inundated, thus causing large areas submerged in these parts ([Al Jazeera, 6 September 2022](#)). Nigeria and Niger saw the earliest onset of large floods in the first half of June, followed by Chad in July, Cameroon in August, and finally, Benin in September ([Sahara Reporters, 2022](#); [Africa News, 2022](#); [Reliefweb, 2022a](#); [Reliefweb, 2022b](#); [Davies, 2022](#)).

With at least 612 and 195 fatalities, respectively, the floods over Nigeria and Niger are among the deadliest in the countries' history ([Africa News, 2022](#); [Ruth, 2022](#); [Akbarzai et al. 2022](#)). The devastation in Nigeria is worse than the 2012 flood disaster ([Balogun et al. 2021](#)) with 34 out of 36 states and over 3.2 million people affected, including 1.5 million displaced and 2.776 injured ([Telesur English, 2022](#); [The Conversation, 2022](#); [Punch, 2022](#); [Addeh, Ajimotokan and Uzoho, 2022](#)). Several hundreds of thousands of hectares of land have been inundated, causing damage to more than 300 thousand homes and over half a million hectares of farmland ([Telesur English, 2022](#); [Asadu, 2022](#)). Home to at least 108 fatalities, the Minister of Humanitarian Affairs, Disaster Management, and Social Development has identified the state of Jigawa as worst affected following several flash floods over the rainy season ([Channels TV, 2022](#); [Maishanu, 2022](#)). In Niger, the number of flood affected people has reached at least 327,000, and over 30,000 homes and shelters, six medical centres, 126 classrooms, and 234 grain stores have been damaged or destroyed ([ECHO Daily Flash, 2022a](#); [OCHA, 2022](#)). Further, over 2,303 hectares of crops have flooded and nearly 700 cattle died, impacting the already precarious livelihoods of many.

Following the heaviest rains in three decades, Chad declared a State of Emergency on 19 October ([France24, 2022](#)). Out of the country's over 1.1 million affected people, nearly half (442,000) of whom are displaced, and 22 have died, across 18 out of the 23 provinces ([REFL, 2022](#); [CARE, 2022](#); [Reuters, 2022](#); [OCHA, 2022](#)). At least 56,607 homes, 465,000 hectares of crops, and numerous roads and bridges have been destroyed, with 1,112 water points and wells disrupted ([IFRC, 2022](#); [ECHO Daily Flash, 2022b](#); [CARE, 2022](#)).

The lingering floodwaters, coupled with disrupted water, sanitation and hygiene (WaSH) services, have been causing new disease outbreaks and aggravating existing ones in the affected countries. From January through September, cholera took 256 lives in Nigeria ([Outbreak News Today, 2022](#)). Since September, the water-borne disease has spread and is now plaguing the borderlands around Nigeria, Niger, Chad, and Cameroon, and has killed at least another 17 people ([Kindzeka, 2022](#); [Reliefweb, 2022c](#)). Vector-borne diseases such as malaria and yellow fever have also increased following the onset of the West African rainy season ([WHO, 2022](#); [OCHA, 2022](#)).

The West African Monsoon circulation is driven by thermodynamic contrast between the cooler ocean (the equatorial Atlantic) and an intense heat low (the Saharan Heat Low) that develops over the western Sahara during the boreal summer. South-westerly winds are established between the equatorial Atlantic and the Saharan Heat Low, bringing moisture into the continent ([Nicholson, 2013](#)). Within the monsoon there are two areas of peak moisture flux convergence and vertical motion; the dominant region lies around 10°N in August, and is associated with the core of the rainbelt and deep meridional overturning. The second region of ascent further north (20°N in August) is weaker, with shallower overturning. The InterTropical Front (ITF) marks the boundary between the warm moist southwesterly monsoon flow to the south and the hotter and drier northeasterly Harmattan winds from the Sahara Desert ([Lele and Lamb, 2010](#)), and represents the northern extent of the West African Monsoon. The ITF advances north from April to early August, and retreats south from August to November; during the early advance and late retreat stages, rainfall over the Sahel is positively correlated with the ITF's latitude ([Lele and Lamb, 2010](#)).

The African Easterly Jet (AEJ), also driven by the low-level temperature gradient from the Gulf of Guinea to the Sahara Desert, is characterized by a peak in the zonal easterly wind at 600–700 hPa over West Africa ([Cornforth et al., 2017](#)). African Easterly Waves are synoptic-scale disturbances that propagate westward on the AEJ, from central or eastern Africa across West Africa and into the tropical Atlantic ([Cornforth et al., 2017](#)). Their passage is marked by a peak in convection and precipitation ([Cornforth et al., 2017](#)).

The 2022 rainy season was characterised by mixed conditions over West Africa, with the seasonal rainfall ranging from below-normal to above-normal in different regions ([Reliefweb, 27 September 2022](#)), resulting in floods in these parts at different times during the season. Therefore, we define this event over two regions where the impacts were maximum. The first region is defined over the Lake Chad basin where the entire JJAS period was characterised by wetter-than-normal conditions. For this region, the event is defined by the JJAS average rainfall, area-averaged over the basin (Fig. 1(a)). The second region, hereafter called Lower Niger, comprises the Lower Niger basin, the Abonyi river basin, and part of the Middle Niger region that lies within Nigeria; this region contains the Lagdo dam, which contributed to downstream flooding in Nigeria when the dam was opened on September 20th ([Reliefweb, 2022d](#); [Voice of Nigeria, 2022](#)). The event is defined by the maximum 7-day rainfall area-averaged over this region (Fig. 1(b)).

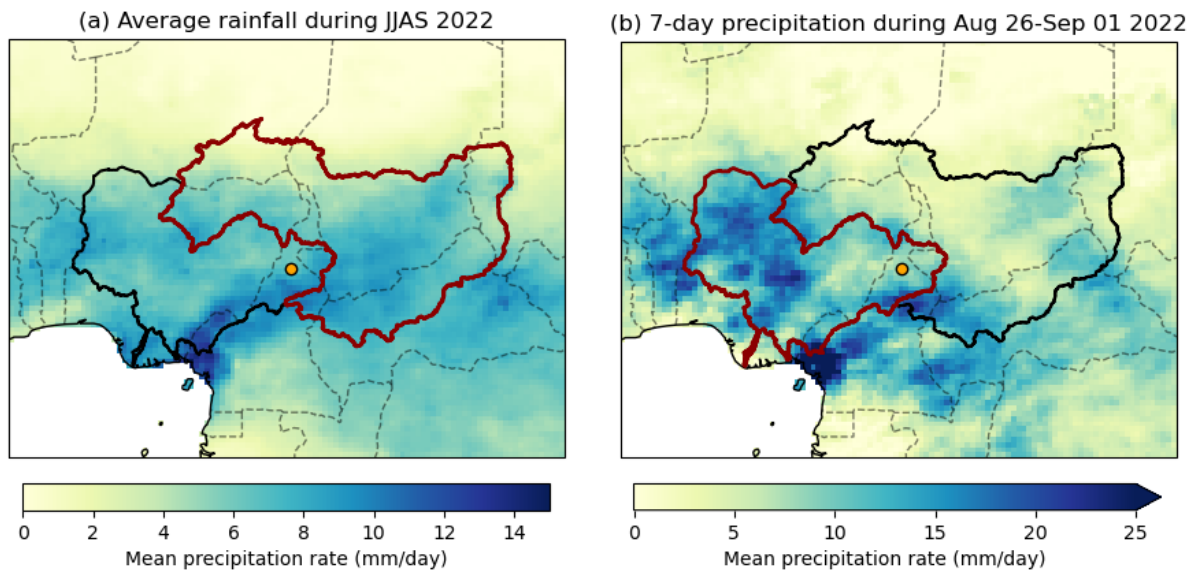


Fig. 1 a) Observed average JJAS rainfall in the year 2022. The red highlight shows the Lake Chad catchment (b) Observed mean daily precipitation from 26 Aug-1 Sep, 2022, the wettest 7-day period over the Lower Niger catchment in JJAS 2022. The red highlight shows the Lower Niger catchment. The location of the Lagdo Dam is marked with an orange dot in both panels, and national borders with dashed lines. Observations are taken from the CHIRPS dataset described in Section 2.1.

Above-normal rainy seasons in West Africa are often accompanied by widespread floods, with previous major impactful events having occurred in the years 1999 and 2012 ([Badou et al., 2019](#)). Most regions of West Africa saw comparably wet years in the mid-20th century followed by very dry years in the 1970s and 1980s that is attributed to aerosol cooling of the Northern Hemisphere which had shifted the ITCZ further south ([IPCC, 2021](#)). More recently more rainfall is observed in most parts of the region with more intense extreme events that is partly explained by the combined effects of increasing greenhouse gas concentrations and decreasing anthropogenic aerosols over Europe and North America shifting the ITCZ back north ([Dong and Sutton, 2015](#), [IPCC, 2021](#)). This increase in the frequency of heavy rains was also assessed by recent studies ([Taylor et al. 2017](#); [Panthou et al. 2014](#)) which depicted more intense Sahelian storms since the 1980s using 35 years of satellite observations and rain gauges in the region. Both observation and modeling studies ([Taylor et al. 2017](#); [Panthou et al. 2014](#); [Sultan et al. 2019](#)) attributed this intensification of the rains to global warming, which particularly affects the temperatures in the Sahara. A warmer Sahara intensifies convection within Sahelian storms through increased wind shear and changes to the Saharan air layer ([Berg et al. 2013](#)) leading to more intense heavy precipitation.

[The most recent IPCC](#) further notes that tropical sea surface temperatures and associated dynamical changes could increase rainfall in West Africa. Rainfall projections are however uncertain because of contrasting signals from models with especially large discrepancies over the main rainy season ([Dosio et al., 2019](#)), with the uncertainty mostly linked to the dynamical response, rather than the thermodynamic response of models ([Monerie et al., 2020](#)).

2 Data and methods

2.1 Observational data

We use two gridded datasets for fitting probability distributions to rainfall in the study regions and for analysing the wetter than normal rainfall event of 2022 in the context of climate change. The first dataset used in the study is the rainfall product from UC Santa Barbara Climate Hazards Group called “Climate Hazards Group InfraRed Precipitation with Station data” (CHIRPS; Funk et al. 2015). The second dataset is the rainfall product developed by the Tropical Applications of Meteorology using SATellite data and ground-based observations (TAMSAT) group at the University of Reading, UK that is based on high-resolution Meteosat thermal infrared (TIR) imagery that are calibrated using rain gauge observations (Maidment et al., 2014, 2017; Tarnavsky, 2014). These datasets start in the years 1981 and 1983 respectively, and have wide applications in weather monitoring and forecasting and crises management in Africa by engaging with the various government agencies (see <http://www.tamsat.org.uk/impact>; <https://www.chc.ucsb.edu/monitoring>). Fig. 2 shows the time series of the average JJAS rainfall in the Lake Chad catchment (Fig. 2(a) and the maximum 7-day rainfall over Lower Niger (Fig. 2 (b)). Panel (a) shows a clear increasing trend in JJAS over the Lake Chad catchment, suggestive of climate change; in panel (b) the trend in 7-day precipitation events is less clear, although the CHIRPS dataset indicates an increase. The differences in the trends between the datasets can be partially ascribed to the differences in their respective algorithms.

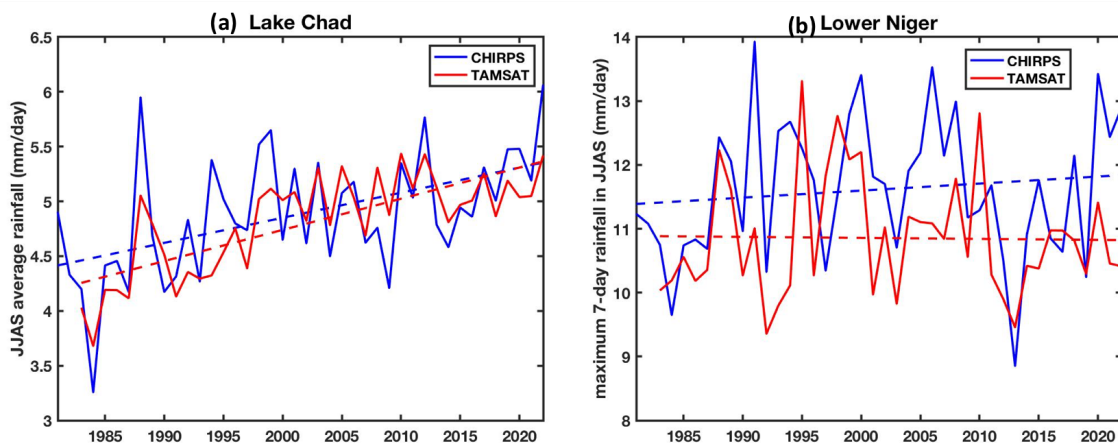


Fig. 2 Time series of (a) average JJAS rainfall over Lake Chad catchment and (b) maximum 7-day rainfall over Lower Niger, based on CHIRPS and TAMSAT.

As a measure of anthropogenic climate change we use the (low-pass filtered) global mean surface temperature anomalies (GMST), where GMST is taken from the National Aeronautics and Space Administration (NASA) Goddard Institute for Space Science (GISS) surface temperature analysis (GISTEMP, [Hansen et al., 2010](#) and [Lenssen et al., 2019](#)).

2.2 Model and experiment descriptions

For this study, we use three multi-model ensembles from climate modelling experiments using very different framings ([Philip et al., 2020](#)): Sea Surface temperature (SST) driven global circulation high resolution models and coupled global circulation models.

The first ensemble comes from the CORDEX-Africa multi-model ensemble at 0.44° resolution (AFR-44; [Nikulin et al., 2012](#)) and 0.22° resolution (AFR-22; [Remedio et al., 2019](#)), comprising of

39 simulations resulting from pairings of Global Climate Models (GCMs) and Regional Climate Models (RCMs). These simulations are composed of historical simulations up to 2005, and extended to the year 2100 using the RCP8.5 scenario. These regional climate models have been widely evaluated over Africa. They capture the occurrence of the West African Monsoon jump and the timing and amplitude of the mean annual cycle of precipitation and temperature over the homogeneous sub-regions of West Africa (Gbobaniyi et al., 2014),

The second ensemble considered in this study is the HighResMIP SST-forced model ensemble ([Haarsma et al., 2016](#)), the simulations for which span from 1950 to 2050. The SST and sea ice forcings for the period 1950-2014 are obtained from the 0.25° x 0.25° Hadley Centre Global Sea Ice and Sea Surface Temperature dataset that have undergone area-weighted regridding to match the climate model resolution. For the ‘future’ time period (2015-2050), SST/sea-ice data are derived from RCP8.5 (CMIP5) data, and combined with greenhouse gas forcings from SSP5-8.5 (CMIP6) simulations (see Section 3.3 of [Haarsma et al., 2016](#) for further details).

The third ensemble comes from the CMIP6 project ([Eyring et al., 2016](#)). For all simulations, the period 1850 to 2015 is based on historical simulations, while the SSP5-8.5 scenario is used for the remainder of the 21st century.

2.3 Statistical methods

In this report we analyse time series from the Lake Chad region for JJAS mean precipitation and from the Lower Niger region for maximum 7-day precipitation values. Methods for observational and model analysis and for model evaluation and synthesis are used according to the World Weather Attribution Protocol, described in Philip et al. (2020), with supporting details found in van Oldenborgh et al. (2021), Ciavarella et al. (2021) and [here](#).

The analysis steps include: (i) trend calculation from observations; (ii) model validation; (iii) multi-method multi-model attribution and (iv) synthesis of the attribution statement.

We calculate the return periods, Probability Ratio (PR; the factor-change in the event's probability) and change in intensity of the event under study in order to compare the climate of now and the climate of the past, defined respectively by the GMST values of now and of the preindustrial past (1850-1900, based on the Global Warming Index <https://www.globalwarmingindex.org>). To statistically model the event under study, we use a Gaussian distribution that scales with GMST for the JJAS series and a GEV distribution that scales with GMST for the maximum 7-day precipitation series. Next, results from observations and models that pass the validation tests are synthesized into a single attribution statement.

3 Observational analysis: return period and trend

3.1 Analysis of gridded data

Fig. 3 shows the trend fitting methods described in Philip et al. (2020) applied to the JJAS average rainfall, area-averaged over Lake Chad (Fig. 1(a)) based on CHIRPS (Fig. 3(a)) and TAMSAT datasets (Fig. 3(b)). The left panels show the variable as a function of the GMST anomaly, while the right panels show the Gaussian distribution-based return period curves for this variable in the present 2022 climate (red lines) and the past climate when the global mean temperature was 1.2°C cooler (blue lines) for the respective datasets.

The seasonal rainfall over Lake Chad is found to increase significantly due to rising global temperatures. This signal is evident in both datasets (Fig. 3(a,c)). The return period of the 2022 JJAS average rainfall in the 2022 climate is 13 years, based on the CHIRPS dataset. This value is much smaller from the TAMSAT data, about 2 years. It may be noted that neither datasets are not long enough to get return period estimates with enough confidence. Therefore, we round these to a more conservative 1-in-10 years for this catchment. The probability ratio with respect to the hypothetical 1.2°C cooler climate is found to be high (>10000) for both datasets, with rainfall increases of 30% and 40% in the current climate, from CHIRPS and TAMSAT datasets, respectively.

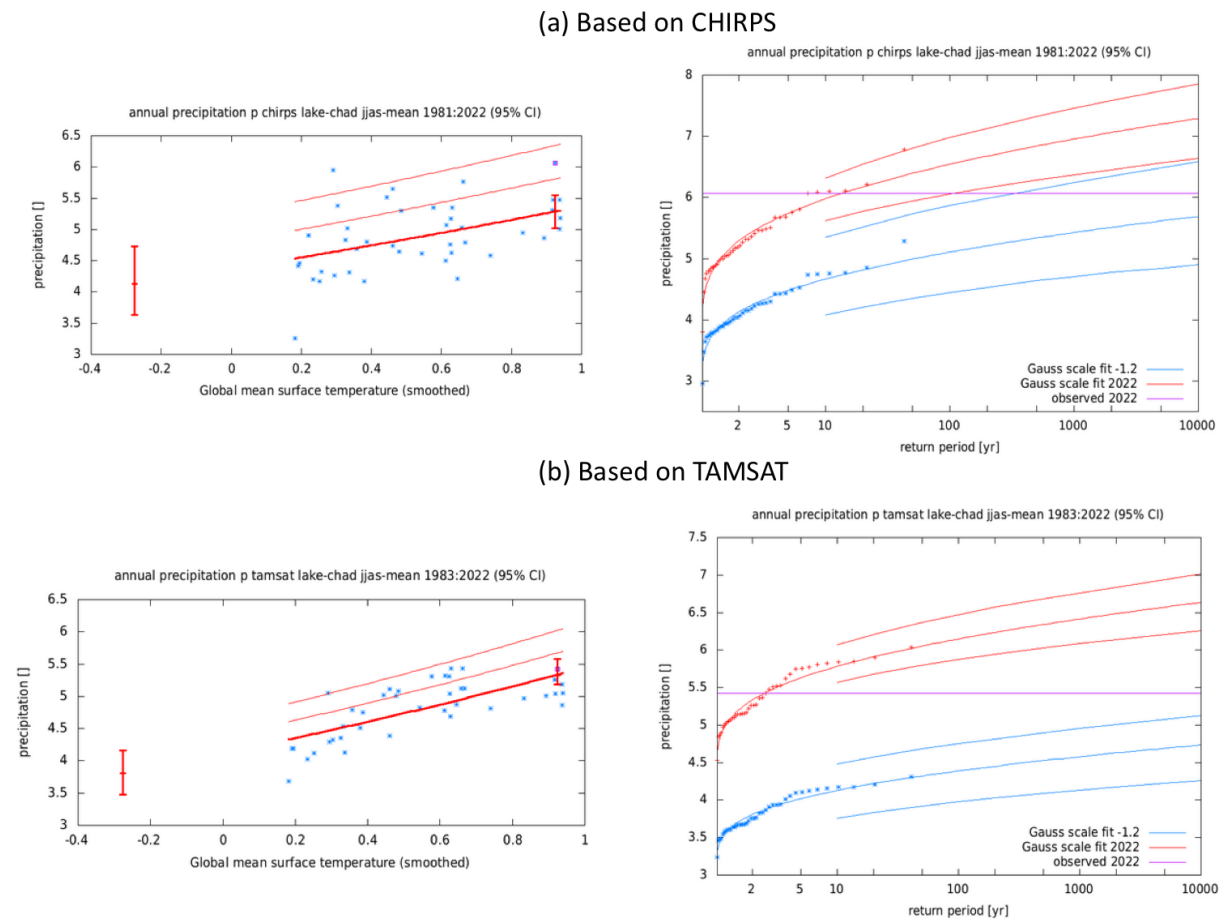
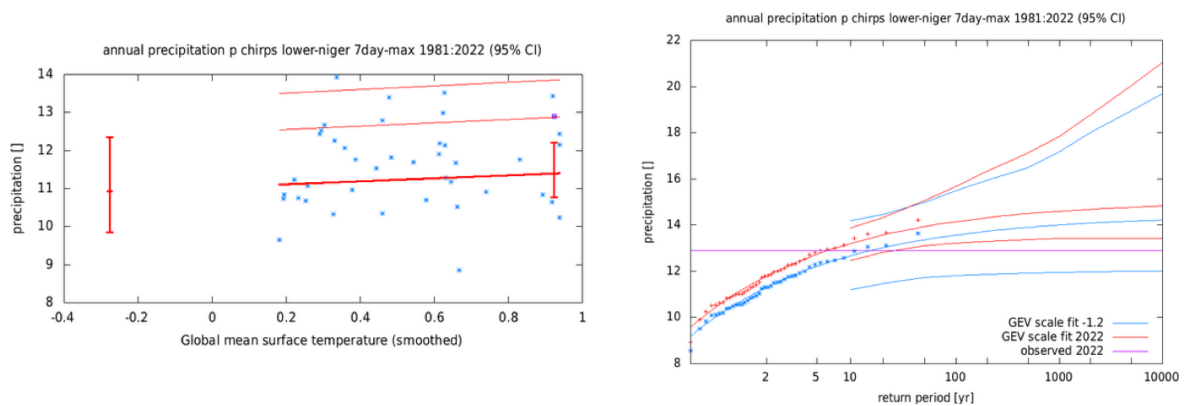


Fig. 3 Gaussian fit with constant dispersion parameter, and location parameter scaled proportional to observed GMST, for the Lake Chad catchment based on two gridded datasets- (a) CHIRPS and (b) TAMSAT. The 2022 event is included in the fit. Left: Observed JJAS average rainfall as a function of the smoothed GMST. The thick red line denotes the time-varying location parameter. The vertical red lines show the 95% confidence interval for the location parameter, for the current, 2022 climate and a 1.2°C cooler climate. The 2022 observation is

highlighted with the magenta box. **Right:** Return time plots for the climate of 2022 (red) and a climate with GMST 1.2 °C cooler (blue). The past observations are shown twice: once shifted up to the current climate and once shifted down to the climate of the late nineteenth century. The markers show the data and the lines show the fits and uncertainty from the bootstrap. The magenta line shows the magnitude of the 2022 event analysed here.

Fig. 4 shows similar plots for maximum 7-day rainfall during JJAS season, averaged over the Lower Niger region (Fig. 1(b)). Despite the high inter-annual variability (Fig. 2(b)), there is a climate change signal in the 7-day rainfall, in both datasets (Fig. 4 (a,c)). The return period of the 2022 event in the present climate are 6 and 1 year(s) based on the CHIRPS and TAMSAT data (Fig. 5(b,d)); we round these to 1-in-5 years for subsequent analysis. The event is found to have been made 2 times more likely (PR=2) and 4-5% intense by climate change.

(a) Based on CHIRPS



(b) Based on TAMSAT

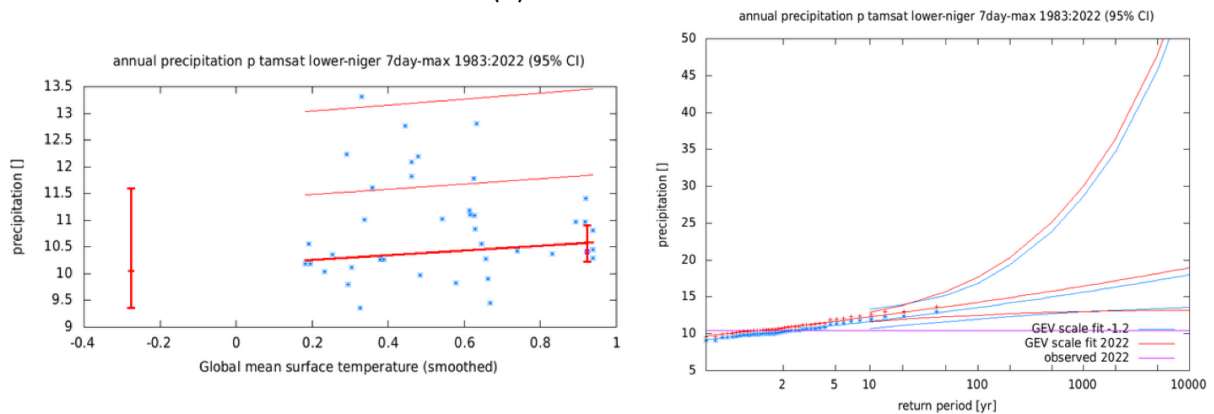


Fig. 4 GEV fit with constant dispersion and shape parameters, and location parameter scaled proportional to observed GMST, for the Lower Niger catchment based on two gridded datasets- (a) CHIRPS and (b) TAMSAT. The 2022 event is included in the fit. **Left:** Observed JJAS average rainfall as a function of the smoothed GMST. The thick red line denotes the time-varying location parameter. The vertical red lines show the 95% confidence interval for the location parameter, for the current, 2022 climate and a 1.2°C cooler climate. The 2022 observation is highlighted with the magenta box. **Right:** Return time plots for the climate of 2022 (red) and a climate with GMST 1.2 °C cooler (blue). The past observations are shown twice: once shifted up to the current climate and once shifted down to the climate of the late nineteenth century. The markers show the data and the lines show the fits and uncertainty from the bootstrap. The magenta line shows the magnitude of the 2022 event analysed here.

and the lines show the fits and uncertainty from the bootstrap. The magenta line shows the magnitude of the 2022 event analysed here.

4 Model evaluation

In the subsections below we show the results of the model validation for the Lake Chad (Table 1) and Lower Niger regions (Table 2) . Per framing or model setup we use models that only just pass the validation tests. if we only have five models or less for that framing that performs well. The climate models are evaluated against the observations in their ability to capture:

1. Seasonal cycles: For this, we qualitatively compare the model outputs against observations-based plots. We discard the models that exhibit multi-modality and/or ill-defined peaks in their seasonal cycles. We also discard the model if the rainy season onset/termination varies significantly from the observations.
2. Spatial patterns: Models that do not match the observations in terms of the large-scale precipitation patterns are excluded.
3. Parameters of the fitted Gaussian/GEV models. We discard the model if the model and observation parameters ranges do not overlap.

The models are labelled as ‘good’, ‘reasonable’, or ‘bad’ based on their performances in terms of the three criteria discussed above.

Table 1. Evaluation results of the climate models considered for attribution analysis of the seasonal rainfall over Lake Chad. The table consists of qualitative assessments of the seasonal cycles and spatial patterns, dispersion parameter a from fitting a Gaussian distribution that scales with time and the magnitude of the 1-in- 10 year event in the 2022 climate.

Observations	Seasonal cycle	Spatial pattern	Dispersion	Event magnitude [mm]
CHIRPS (1981-2022)			0.102 (0.0740 ... 0.123)	38.53
TAMSAT(1983-2022)			0.0660 (0.0520 ... 0.0750)	38.373
Model				Threshold for 10-yr return period
CNRM-CM5_r1_CCLM4-8-17 hist-rcp85 (AFR-44)	bad	bad	<not computed>	<not computed>
CNRM-CM5_r1_RCA4 hist-rcp85 (AFR-44)	reasonable	bad	<not computed>	<not computed>
CSIRO-Mk3-6-0_r1_RCA4 hist-rcp85 (AFR-44)	bad	bad	<not computed>	<not computed>
CanESM2_r1_CanRCM4 hist-rcp85 (AFR-44)	reasonable	bad	<not computed>	<not computed>
CanESM2_r1_RCA4 hist-rcp85 (AFR-44)	reasonable	bad	<not computed>	<not computed>

EC-EARTH_r12_CCLM4-8-17 hist-rcp85 (AFR-44)	bad	bad	<not computed>	<not computed>
EC-EARTH_r12_RCA4 hist-rcp85 (AFR-44)	bad	bad	<not computed>	<not computed>
EC-EARTH_r12_REMO2009 hist-rcp85 (AFR-44)	good	good	0.165 (0.126 ... 0.193)	4.67
EC-EARTH_r1_RACMO22T hist-rcp85 (AFR-44)	reasonable	bad	<not computed>	<not computed>
EC-EARTH_r1_RCA4 hist-rcp85 (AFR-44)	bad	bad	<not computed>	<not computed>
EC-EARTH_r3_HIRHAM5 hist-rcp85 (AFR-44)	good	bad	<not computed>	<not computed>
EC-EARTH_r3_RCA4 hist-rcp85 (AFR-44)	bad	bad	<not computed>	<not computed>
GFDL-ESM2M_r1_RCA4 hist-rcp85 (AFR-44)	bad	bad	<not computed>	<not computed>
HadGEM2-ES_r1_CCLM4-8-17 hist-rcp85 (AFR-44)	reasonable	reasonable	<not computed>	<not computed>
HadGEM2-ES_r1_RACMO22T hist-rcp85 (AFR-44)	bad	bad	<not computed>	<not computed>
HadGEM2-ES_r1_RCA4 hist-rcp85 (AFR-44)	reasonable	bad	<not computed>	<not computed>
HadGEM2-ES_r1_REMO2009 hist-rcp85 (AFR-44)	good	good	0.134 (0.0960 ... 0.165)	6.39
HadGEM2-ES_r1_RegCM4-3 hist-rcp85 (AFR-44)	good	reasonable	0.102 (0.0810 ... 0.120)	6.36
IPSL-CM5A-LR_r1_REMO2009 hist-rcp85 (AFR-44)	good	good	0.148 (0.117 ... 0.171)	3.60
IPSL-CM5A-MR_r1_RCA4 hist-rcp85 (AFR-44)	good	bad	<not computed>	<not computed>
MIROC5_r1_RCA4 hist-rcp85 (AFR-44)	reasonable	bad	<not computed>	<not computed>
MIROC5_r1_REMO2009 hist-rcp85 (AFR-44)	good	good	0.164 (0.125 ... 0.193)	5.45
MPI-ESM-LR_r1_CCLM4-8-17 hist-rcp85 (AFR-44)	bad	good	<not computed>	<not computed>
MPI-ESM-LR_r1_RCA4 hist-rcp85 (AFR-44)	reasonable	bad	<not computed>	<not computed>
MPI-ESM-LR_r1_REMO2009 hist-rcp85 (AFR-44)	good	good	0.142 (0.109 ... 0.167)	4.44
MPI-ESM-LR_r2_RCA4 hist-rcp85 (AFR-44)	reasonable	bad	<not computed>	<not computed>
MPI-ESM-LR_r3_RCA4 hist-rcp85 (AFR-44)	reasonable	bad	<not computed>	<not computed>
MPI-ESM-MR_r1_RegCM4-3 hist-rcp85 (AFR-44)	reasonable	good	0.102 (0.0760 ... 0.123)	5.84
NorESM1-M_r1_RCA4 hist-rcp85 (AFR-44)	bad	bad	<not computed>	<not computed>

CanESM2_r1_CanRCM4 hist-rcp85 (AFR-22)	bad	bad	<not computed>	<not computed>
HadGEM2-ES_r1_CCLM5-0-15 hist-rcp85 (AFR-22)	bad	reasonable	<not computed>	<not computed>
HadGEM2-ES_r1_REMO2015 hist-rcp85 (AFR-22)	good	reasonable	0.116 (0.0830 ... 0.149)	6.33
HadGEM2-ES_r1_RegCM4-7 hist-rcp85 (AFR-22)	good	good	0.162 (0.127 ... 0.190)	9.03
MPI-ESM-LR_r1_CCLM5-0-15 hist-rcp85 (AFR-22)	bad	bad	<not computed>	<not computed>
MPI-ESM-LR_r1_REMO2015 hist-rcp85 (AFR-22)	reasonable	bad	<not computed>	<not computed>
MPI-ESM-MR_r1_RegCM4-7 hist-rcp85 (AFR-22)	reasonable	good	0.161 (0.124 ... 0.188)	6.27
NorESM1-M_r1_CCLM5-0-15 hist-rcp85 (AFR-22)	bad	reasonable	<not computed>	<not computed>
NorESM1-M_r1_REMO2015 hist-rcp85 (AFR-22)	good	bad	<not computed>	<not computed>
NorESM1-M_r1_RegCM4-7 hist-rcp85 (AFR-22)	reasonable	good	0.215 (0.172 ... 0.248)	<not computed>
CMCC-CM2-VHR5 HighResMIP (1)	reasonable	good	0.0710 (0.0510 ... 0.0860)	6.89
CNRM-CM6-1-HR HighResMIP (1)	reasonable	reasonable	0.370 (0.276 ... 0.440)	2.87
EC-Earth3P-HR HighResMIP (1)	good	good	0.102 (0.0770 ... 0.120)	6.24
HadGEM3-GC31-HM HighResMIP (1)	good	good	0.0920 (0.0690 ... 0.110)	6.07
HadGEM3-GC31-MM HighResMIP (1)	good	good	0.108 (0.0860 ... 0.123)	5.63
MPI-ESM1-2-XR HighResMIP (1)	good	reasonable	0.164 (0.121 ... 0.195)	6.07
ACCESS-ESM1-5 CMIP6-ssp585 (1)	good	good	0.0850 (0.0700 ... 0.0960)	< not computed>
CanESM5 CMIP6-ssp585 (1)	bad	good	0.0990 (0.0840 ... 0.112)	< not computed>
CMCC-ESM2 CMIP6-ssp585 (1)	reasonable	reasonable	0.0760 (0.0610 ... 0.0890)	< not computed>
CNRM-CM6-1-HR CMIP6-ssp585 (1)	bad		0.135 (0.110 ... 0.156)	< not computed>
CNRM-CM6-1 CMIP6-ssp585 (1)	reasonable	bad	0.196 (0.160 ... 0.225)	< not computed>
CNRM-ESM2-1 CMIP6-ssp585 (1)	good	reasonable	0.170 (0.132 ... 0.202)	< not computed>
GFDL-CM4 CMIP6-ssp585 (1)	bad	good	0.0990 (0.0830 ... 0.114)	< not computed>
IPSL-CM6A-LR CMIP6-ssp585 (1)	good	good	0.0830 (0.0670 ... 0.0940)	< not computed>
MIROC6 CMIP6-ssp585 (1)	bad	bad	0.102 (0.0850 ... 0.116)	< not computed>

MPI-ESM1-2-HR CMIP6-ssp585 (1)	reasonable	reasonable	0.105 (0.0860 ... 0.120)	< not computed>
MPI-ESM1-2-LR CMIP6-ssp585 (1)	reasonable	reasonable	0.116 (0.0990 ... 0.128)	< not computed>
NorESM2-LM CMIP6-ssp585 (1)	reasonable	reasonable	0.126 (0.0990 ... 0.150)	< not computed>

Table 2. Evaluation results of the climate models considered for attribution analysis of the seasonal rainfall over Lower Niger. The table consists of qualitative assessments of the seasonal cycles and spatial patterns, dispersion parameter a from fitting a GEV distribution that scales with time and the magnitude of the 1-in- 5 year event in the 2022 climate.

Observations	Seasonal cycle	Spatial pattern	Dispersion	Shape	Event magnitude [mm]
CHIRPS (1981-2022)			0.0980 (0.0620 ... 0.124)	-0.30 (-0.67 ... 0.056)	38.53
TAMSAT(1983-2022)			0.0670 (0.0430 ... 0.0900)	0.052 (-0.28 ... 0.40)	38.373
Model					Threshold for 5-yr return period
CNRM-CM5_r1_CCLM4-8-17 hist-rcp85 (AFR-44)	bad	bad	< not computed>	< not computed>	< not computed>
CNRM-CM5_r1_RCA4 hist-rcp85 (AFR-44)	good	bad	< not computed>	< not computed>	< not computed>
CSIRO-Mk3-6-0_r1_RCA4 hist-rcp85 (AFR-44)	bad	bad	< not computed>	< not computed>	< not computed>
CanESM2_r1_CanRCM4 hist-rcp85 (AFR-44)	bad	bad	< not computed>	< not computed>	< not computed>
CanESM2_r1_RCA4 hist-rcp85 (AFR-44)	bad	bad	< not computed>	< not computed>	< not computed>
EC-EARTH_r12_CCLM4-8-17 hist-rcp85 (AFR-44)	bad	bad	< not computed>	< not computed>	< not computed>
EC-EARTH_r12_RCA4 hist-rcp85 (AFR-44)	bad	bad	< not computed>	< not computed>	< not computed>
EC-EARTH_r12_REMO2009 hist-rcp85 (AFR-44)	bad	bad	0.155 (0.124 ... 0.173)	-0.35 (-0.53 ... -0.11)	13.993
EC-EARTH_r1_RACMO22T hist-rcp85 (AFR-44)	bad	bad	< not computed>	< not computed>	< not computed>
EC-EARTH_r1_RCA4 hist-rcp85 (AFR-44)	bad	bad	< not computed>	< not computed>	< not computed>
EC-EARTH_r3_HIRHAM5 hist-rcp85 (AFR-44)	good	bad	< not computed>	< not computed>	< not computed>
EC-EARTH_r3_RCA4 hist-rcp85 (AFR-44)	bad	bad	< not computed>	< not computed>	< not computed>
GFDL-ESM2M_r1_RCA4 hist-rcp85 (AFR-44)	bad	bad	< not computed>	< not computed>	< not computed>
HadGEM2-ES_r1_CCLM4-8-17 hist-rcp85 (AFR-44)	bad		< not computed>	< not computed>	< not computed>
HadGEM2-ES_r1_RACMO22T hist-rcp85 (AFR-44)	bad	bad	< not computed>	< not computed>	< not computed>

HadGEM2-ES_r1_RCA4 hist-rcp85 (AFR-44)	bad	bad	< not computed>	< not computed>	< not computed>
HadGEM2-ES_r1_REMO2009 hist-rcp85 (AFR-44)	good	good	0.205 (0.141 ... 0.243)	-0.24 (-0.45 ... 0.0080)	17.721
HadGEM2-ES_r1_RegCM4-3 hist-rcp85 (AFR-44)	good	reasonable	0.179 (0.133 ... 0.220)	0.10 (-0.092 ... 0.26)	17.081
IPSL-CM5A-LR_r1_REMO2009 hist-rcp85 (AFR-44)	good	good	0.213 (0.162 ... 0.245)	-0.087 (-0.25 ... 0.098)	11.978
IPSL-CM5A-MR_r1_RCA4 hist-rcp85 (AFR-44)	bad	bad	< not computed>	< not computed>	< not computed>
MIROC5_r1_RCA4 hist-rcp85 (AFR-44)	reasonable	bad	< not computed>	< not computed>	< not computed>
MIROC5_r1_REMO2009 hist-rcp85 (AFR-44)	good	good	0.239 (0.172 ... 0.273)	-0.13 (-0.38 ... 0.23)	21.282
MPI-ESM-LR_r1_CCLM4-8-17 hist-rcp85 (AFR-44)	bad	good	< not computed>	< not computed>	< not computed>
MPI-ESM-LR_r1_RCA4 hist-rcp85 (AFR-44)	reasonable	bad	< not computed>	< not computed>	< not computed>
MPI-ESM-LR_r1_REMO2009 hist-rcp85 (AFR-44)	good	good	0.203 (0.152 ... 0.234)	-0.074 (-0.30 ... 0.051)	15.419
MPI-ESM-LR_r2_RCA4 hist-rcp85 (AFR-44)	reasonable	bad	< not computed>	< not computed>	< not computed>
MPI-ESM-LR_r3_RCA4 hist-rcp85 (AFR-44)	reasonable	bad	< not computed>	< not computed>	< not computed>
MPI-ESM-MR_r1_RegCM4-3 hist-rcp85 (AFR-44)	good	good	0.170 (0.127 ... 0.199)	-0.14 (-0.35 ... 0.041)	13.683
NorESM1-M_r1_RCA4 hist-rcp85 (AFR-44)	bad	bad	< not computed>	< not computed>	< not computed>
CanESM2_r1_CanRCM4 hist-rcp85 (AFR-22)	bad	bad	< not computed>	< not computed>	< not computed>
HadGEM2-ES_r1_CCLM5-0-15 hist-rcp85 (AFR-22)	bad	reasonable	< not computed>	< not computed>	< not computed>
HadGEM2-ES_r1_REMO2015 hist-rcp85 (AFR-22)	good	reasonable	0.170 (0.128 ... 0.193)	-0.14 (-0.38 ... 0.019)	16.217
HadGEM2-ES_r1_RegCM4-7 hist-rcp85 (AFR-22)	bad	good	< not computed>	< not computed>	< not computed>
MPI-ESM-LR_r1_CCLM5-0-15 hist-rcp85 (AFR-22)	reasonable	bad	< not computed>	< not computed>	< not computed>
MPI-ESM-LR_r1_REMO2015 hist-rcp85 (AFR-22)	good	bad	< not computed>	< not computed>	< not computed>
MPI-ESM-MR_r1_RegCM4-7 hist-rcp85 (AFR-22)	good	good	0.0940 (0.0680 ... 0.117)	0.085 (-0.19 ... 0.26)	14.833
NorESM1-M_r1_CCLM5-0-15 hist-rcp85 (AFR-22)	reasonable	reasonable	0.139 (0.105 ... 0.171)	0.071 (-0.12 ... 0.23)	11.29
NorESM1-M_r1_REMO2015 hist-rcp85 (AFR-22)	good	bad	< not computed>	< not computed>	< not computed>
NorESM1-M_r1_RegCM4-7 hist-rcp85 (AFR-22)	reasonable	good	0.126 (0.0810 ... 0.151)	-0.29 (-0.52 ... 0.095)	14.22
CMCC-CM2-VHR5 HighResMIP (1)	bad	good	0.102 (0.0760 ... 0.119)	-0.093 (-0.34 ... 0.090)	22.113

CNRM-CM6-1-HR HighResMIP (1)	good	reasonable	0.113 (0.0810 ... 0.138)	0.056 (-0.13 ... 0.22)	17.921
EC-Earth3P-HR HighResMIP (1)	good	good	0.0870 (0.0650 ... 0.103)	-0.12 (-0.30 ... 0.087)	16.327
HadGEM3-GC31-HM HighResMIP (1)	good	good	0.105 (0.0830 ... 0.119)	-0.23 (-0.43 ... -0.012)	18.215
HadGEM3-GC31-MM HighResMIP (1)	good	good	0.104 (0.0730 ... 0.122)	-0.16 (-0.38 ... 0.026)	17.005
MPI-ESM1-2-XR HighResMIP (1)	good	reasonable	0.111 (0.0810 ... 0.130)	-0.39 (-0.63 ... -0.23)	5.83
ACCESS-ESM1-5 CMIP6-ssp585 (1)	reasonable	good	0.138 (0.110 ... 0.158)	-0.089 (-0.29 ... 0.063)	< not computed>
CanESM5 CMIP6-ssp585 (1)	bad	good	0.183 (0.150 ... 0.215)	-0.42 (-0.67 ... -0.28)	< not computed>
CMCC-ESM2 CMIP6-ssp585 (1)	bad	reasonable	0.111 (0.0900 ... 0.129)	0.11 (-0.047 ... 0.31)	< not computed>
CNRM-CM6-1-HR CMIP6-ssp585 (1)	reasonable	<not evaluated>	0.125 (0.0920 ... 0.147)	-0.060 (-0.38 ... 0.15)	< not computed>
CNRM-CM6-1 CMIP6-ssp585 (1)	reasonable	bad	0.156 (0.107 ... 0.185)	-0.025 (-0.26 ... 0.24)	< not computed>
CNRM-ESM2-1 CMIP6-ssp585 (1)	good	reasonable	0.127 (0.101 ... 0.149)	-0.053 (-0.28 ... 0.22)	< not computed>
GFDL-CM4 CMIP6-ssp585 (1)	bad	good	0.0950 (0.0720 ... 0.109)	0.063 (-0.069 ... 0.25)	< not computed>
IPSL-CM6A-LR CMIP6-ssp585 (1)	good	good	0.136 (0.110 ... 0.157)	-0.062 (-0.24 ... 0.16)	< not computed>
MIROC6 CMIP6-ssp585 (1)	reasonable	bad	0.121 (0.0940 ... 0.143)	-0.16 (-0.41 ... -0.029)	< not computed>
MPI-ESM1-2-HR CMIP6-ssp585 (1)	good	reasonable	0.112 (0.0920 ... 0.128)	-0.14 (-0.36 ... -0.0030)	< not computed>
MPI-ESM1-2-LR CMIP6-ssp585 (1)	reasonable	reasonable	0.0810 (0.0640 ... 0.0940)	-0.087 (-0.32 ... 0.073)	< not computed>
NorESM2-LM CMIP6-ssp585 (1)	bad	reasonable	0.121 (0.0980 ... 0.142)	-0.25 (-0.48 ... -0.12)	< not computed>

5 Multi-method multi-model attribution

This section shows Probability Ratios and change in rain event intensity ΔI for models. Tables 3 and 4 show the model-based results for the models that are labeled ‘reasonable’ or ‘good’.

Table 3. Probability ratio and change in intensity for models that passed the validation tests, for Lake Chad.

Model / Observations	a. Past vs. present		b. Present vs. future	
	Probability ratio PR [-]	Change in intensity ΔI [mm/day]	Probability ratio PR [-]	Change in intensity ΔI [%]
CHIRPS	3.7e+4 (24 ... 2.9e+12)	28 (11 ... 50)		
TAMSAT	8.0e+9 (3.4e+5 ... ∞)	40 (26 ... 60)		
HadGEM2-ES_r1_REMO2009 CORDEX-44_rcp85 ()	18 (4.2 ... 1.0e+2)	16 (7.1 ... 25)	1.6 (0.92 ... 2.7)	2.2 (-0.31 ... 4.8)
HadGEM2-ES_r1_RegCM4-3 CORDEX-44_rcp85 ()	10 (1.7 ... 75)	10 (1.6 ... 20)	2.3 (1.4 ... 4.1)	3.2 (1.2 ... 5.4)

IPSL-CM5A-LR_r1_REMO2009 CORDEX-44_rcp85 ()	3.4 (0.65 ... 15)	7.2 (-2.0 ... 15)	1.5 (1.0 ... 1.9)	2.8 (0.16 ... 5.5)
MPI-ESM-LR_r1_REMO2009 CORDEX-44_rcp85 ()	0.47 (0.12 ... 1.9)	-6.7 (-16 ... 5.3)	0.95 (0.56 ... 1.4)	-0.46 (-4.9 ... 3.3)
MPI-ESM-MR_r1_RegCM4-3 CORDEX-44_rcp85 ()	0.25 (0.058 ... 0.75)	-9.5 (-17 ... -2.0)	0.95 (0.60 ... 1.3)	-0.44 (-3.4 ... 2.3)
HadGEM2-ES_r1_REMO2015 CORDEX-22_rcp85 ()	11 (2.5 ... 1.2e+2)	12 (4.0 ... 22)	1.9 (1.1 ... 3.1)	3.0 (0.28 ... 5.8)
CMCC-CM2-VHR5 HighResMIP (1)	6.6e+2 (35 ... 7.8e+4)	15 (8.6 ... 21)	<not evaluated>	<not evaluated>
EC-Earth3P-HR HighResMIP (1)	1.9e+2 (11 ... 1.0e+4)	18 (9.3 ... 28)	<not evaluated>	<not evaluated>
HadGEM3-GC31-HM HighResMIP (1)	47 (4.9 ... 1.0e+3)	14 (5.4 ... 24)	<not evaluated>	<not evaluated>
HadGEM3-GC31-MM HighResMIP (1)	1.0e+2 (9.2 ... 2.6e+3)	17 (8.1 ... 27)	<not evaluated>	<not evaluated>
ACCESS-ESM1-5 CMIP6-ssp585 (1)	4.8e+3 (5.0e+2 ... 3.3e+5)	22 (15 ... 28)	1.0 (0.76 ... 1.6)	0.15 (... 1.8)
CMCC-ESM2 CMIP6-ssp585 (1)	12 (1.9 ... 3.2e+2)	7.7 (2.3 ... 14)	1.4 (1.1 ... 2.4)	1.7 (0.54 ... 2.7)
IPSL-CM6A-LR CMIP6-ssp585 (1)	44 (7.5 ... 5.8e+2)	12 (5.9 ... 18)	2.2 (1.6 ... 4.4)	4.0 (3.1 ... 4.9)
MPI-ESM1-2-HR CMIP6-ssp585 (1)	6.4e+2 (18 ... 1.4e+5)	22 (9.8 ... 34)	3.5 (2.0 ... 9.1)	8.2 (6.3 ... 10)
MPI-ESM1-2-LR CMIP6-ssp585 (1)	3.4e+2 (14 ... 4.0e+4)	22 (8.8 ... 36)	3.0 (1.9 ... 6.5)	7.8 (5.8 ... 9.7)
NorESM2-LM CMIP6-ssp585 (1)	1.1e+3 (37 ... 4.9e+5)	27 (14 ... 40)	1.2 (0.85 ... 1.8)	1.1 (-1.1 ... 2.9)

Table 4. Probability ratio and change in intensity for models that passed the validation tests, for Lower Niger.

Model / Observations	a. Past vs. present		b. Present vs. future	
	Probability ratio PR [-]	Change in intensity ΔI [%]	Probability ratio PR [-]	Change in intensity ΔI [%]
CHIRPS	2.5 (0.15 ... ∞)	4.3 (-9.5 ... 22)		
TAMSAT	1.6 (0.61 ... 5.2)	5.2 (-11 ... 15)		
EC-EARTH_r12_REMO2009 hist-rcp85 (AFR-44)	0.75 (0.21 ... 2.3)	-3.8 (-16 ... 10)	1.1 (0.79 ... 1.5)	2.0 (-3.7 ... 7.6)
MPI-ESM-MR_r1_RegCM4-3 hist-rcp85 (AFR-44)	0.57 (0.11 ... 1.8)	-7.9 (-24 ... 8.6)	1.0 (0.65 ... 1.4)	0.34 (-5.8 ... 5.1)
MPI-ESM-MR_r1_RegCM4-7 hist-rcp85 (AFR-22)	0.41 (0.17 ... 0.89)	-8.9 (-16 ... -2.3)	1.0 (0.78 ... 1.3)	0.23 (-2.9 ... 3.7)
NorESM1-M_r1_CCLM5-0-15 hist-rcp85 (AFR-22)	0.47 (0.15 ... 1.2)	-11 (-22 ... 3.5)	0.17 (0.043 ... 0.40)	-19 (-27 ... -10)
NorESM1-M_r1_RegCM4-7 hist-rcp85 (AFR-22)	27 (1.6 ... 1.0e+7)	19 (2.7 ... 34)	1.9 (1.1 ... 2.9)	5.5 (0.67 ... 9.5)
EC-Earth3P-HR HighResMIP (1)	46 (3.4 ... ∞)	14 (5.6 ... 23)	<not evaluated>	<not evaluated>
HadGEM3-GC31-HM HighResMIP (1)	6.6 (0.82 ... 2.6e+2)	9.4 (-0.87 ... 18)	<not evaluated>	<not evaluated>
HadGEM3-GC31-MM HighResMIP (1)	57 (3.3 ... ∞)	16 (4.5 ... 27)	<not evaluated>	<not evaluated>
ACCESS-ESM1-5 CMIP6-ssp585 (1)	2.8 (0.84 ... 8.3)	11 (-1.4 ... 21)	1.1 (0.87 ... 1.4)	0.51 (-1.6 ... 2.5)

CNRM-ESM2-1 CMIP6-ssp585 (1)	5.3 (1.2 ... 25)	17 (2.3 ... 29)	1.1 (0.97 ... 1.4)	1.6 (-0.43 ... 3.8)
IPSL-CM6A-LR CMIP6-ssp585 (1)	2.3 (0.90 ... 8.8)	9.1 (-1.1 ... 20)	1.3 (1.1 ... 1.6)	3.2 (1.6 ... 4.8)
MPI-ESM1-2-HR CMIP6-ssp585 (1)	3.3 (0.78 ... 1.6e+4)	9.2 (-2.0 ... 23)	2.2 (1.7 ... 3.7)	8.6 (6.4 ... 11)
MPI-ESM1-2-LR CMIP6-ssp585 (1)	32 (5.4 ... ∞)	20 (11 ... 33)	2.7 (1.7 ... 6.5)	8.9 (7.3 ... 11)

6 Hazard synthesis

For the event definitions described above we evaluate the influence of anthropogenic climate change on the events by calculating the probability ratio as well as the change in intensity using observations and climate models. Models which do not pass the validation tests described above are excluded from the analysis. The aim is to synthesise results from models that pass the evaluation along with the observations-based products, to give an overarching attribution statement. Figs. 5-8 show the changes in probability and intensity for the observations (blue) and models (red). To combine them into a synthesised assessment, first, a representation error is added (in quadrature) to the observations, to account for the difference between observations-based datasets that cannot be explained by natural variability. This is shown in these figures as white boxes around the light blue bars. The dark blue bar shows the average over the observation-based products. Next, a term to account for intermodel spread is added (in quadrature) to the natural variability of the models. This is shown in the figures as white boxes around the light red bars. The dark red bar shows the model average, consisting of a weighted mean using the (uncorrelated) uncertainties due to natural variability plus the term representing intermodel spread (i.e., the inverse square of the white bars). Observation-based products and models are combined into a single result in two ways. Firstly, we neglect common model uncertainties beyond the intermodel spread that is depicted by the model average, and compute the weighted average of models (dark red bar) and observations (dark blue bar): this is indicated by the magenta bar. As, due to common model uncertainties, model uncertainty can be larger than the intermodel spread, secondly, we also show the more conservative estimate of an unweighted, direct average of observations (dark red bar) and models (dark blue bar) contributing 50% each, indicated by the white box around the magenta bar in the synthesis figures.

For the Lake Chad Basin (Fig 5(a)) the observations show a very strong increase in the likelihood of the event occurring that even the data set with the smaller change (CHIRPS) has a lower bound of a probability ratio of 100. There are large discrepancies between the best estimates and overall there are very large uncertainties, which is not unexpected given the high variability of rainfall in the region. Changes in intensity are much more consistent in their magnitude and show an increase of about 30% as the best estimate (Fig. 5(b)). The models show generally much lower trends, and in two cases even negative trends (MPI-ESM-LR_r1_REMO2009 and MPI-ESM-MR_r1_RegCM4-3). Both models with negative trends are from the CORDEX ensemble and all CORDEX models have lower trends. As noted in the introduction, many studies show that aerosol forcing over Europe and North America could play an important role in changing rainfall dynamics over West Africa even though it is unclear whether they play as big a role as greenhouse gasses. Given that aerosols in the CORDEX ensemble are changing in an unrealistic way and different to other ensembles, this could explain the discrepancy in the trend. Generally the uncertainties in models and observations are large, spanning orders of magnitude. However, the large majority of models shows a significant increase in the likelihood of the event occurring which is consistent with the observations. We therefore communicate the best estimate of the weighted synthesis bar, PR of approx. 80, as our overarching result for the change in

likelihood of a 10-year seasonal rainfall event over the Lake Chad Basin. For the change in intensity of the same event the synthesized result is significant with very little discrepancy between the weighted and unweighted average (magenta and white boxes in Fig. 5(b)) despite the negative trends in the models mentioned above. We thus communicate again the best estimate of appr. 20% increase as the overarching result and note that changes in intensity are more robust across models and observations.

Looking at the simulations of potential further changes in a 0.8°C warmer world from today we find a similar picture, with most models apart from the CORDEX ensemble showing a significant increase, albeit smaller than in the past (Fig.6(a-b)). This could imply that indeed aerosol forcing plays an important role in explaining the large increase in likelihood and intensity in the past. However, the models showing the highest increase in the past, the high-res MIP ensemble, are not available at 2°C-simulations, thus the result shown here is probably only the lower bound of possible changes under future warming.

For the Lower Niger Basin event we find qualitatively a similar picture, but overall much smaller trends which are therefore, given the large uncertainties, not significant. The CORDEX models are even more noticeably outliers in the simulations, with NorESM1-M_r1_CCLM5-0-15 showing a strong negative trend (Fig. 7(a)). Given the timescales of the event definition, 7-day seasonal maximum, at which the Clausius Clapeyron relationship holds, we communicate the best estimates, PR of about 2 (Fig. 7(a)) and an increase in intensity if about 5% (Fig. 7(b)), as the overarching results despite the uncertainty range of the synthesised analysis containing no change.

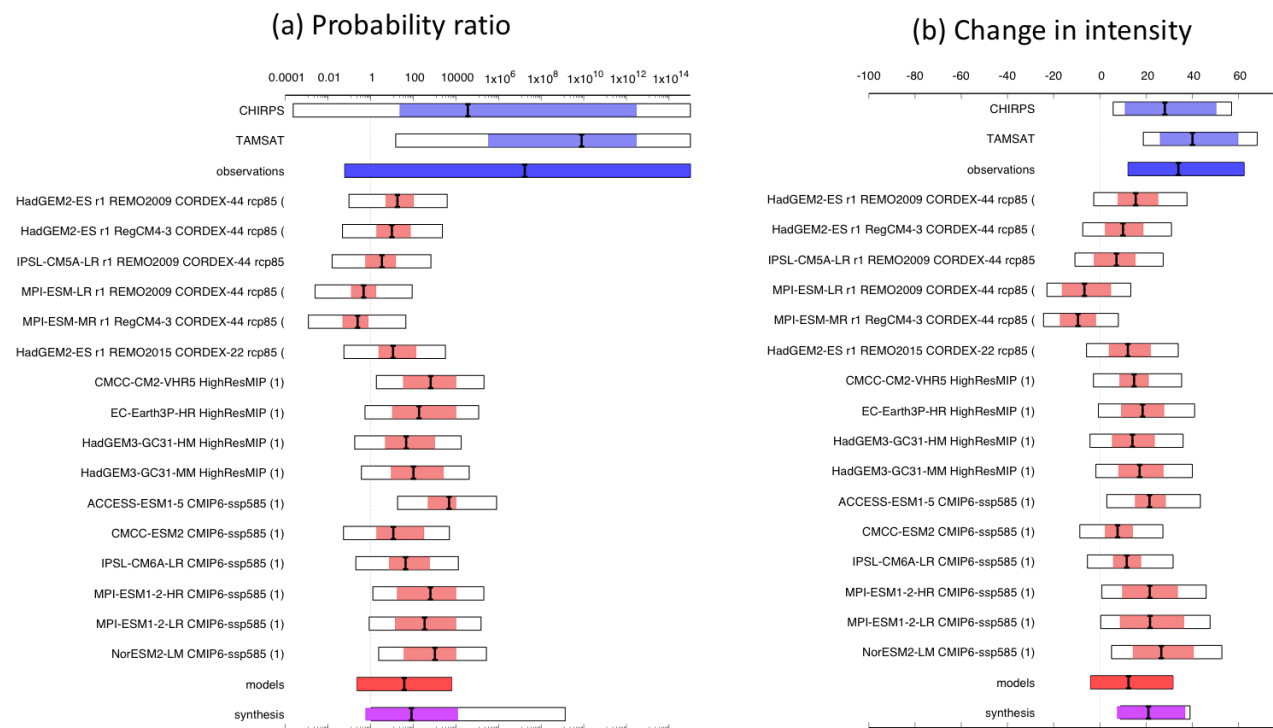


Fig. 5. Synthesis of (a) probability ratios and (b) intensity changes when comparing the return period and magnitudes of the 2022 JJAS seasonal average rainfall over Lake Chad in the current climate and a 1.2°C cooler climate.

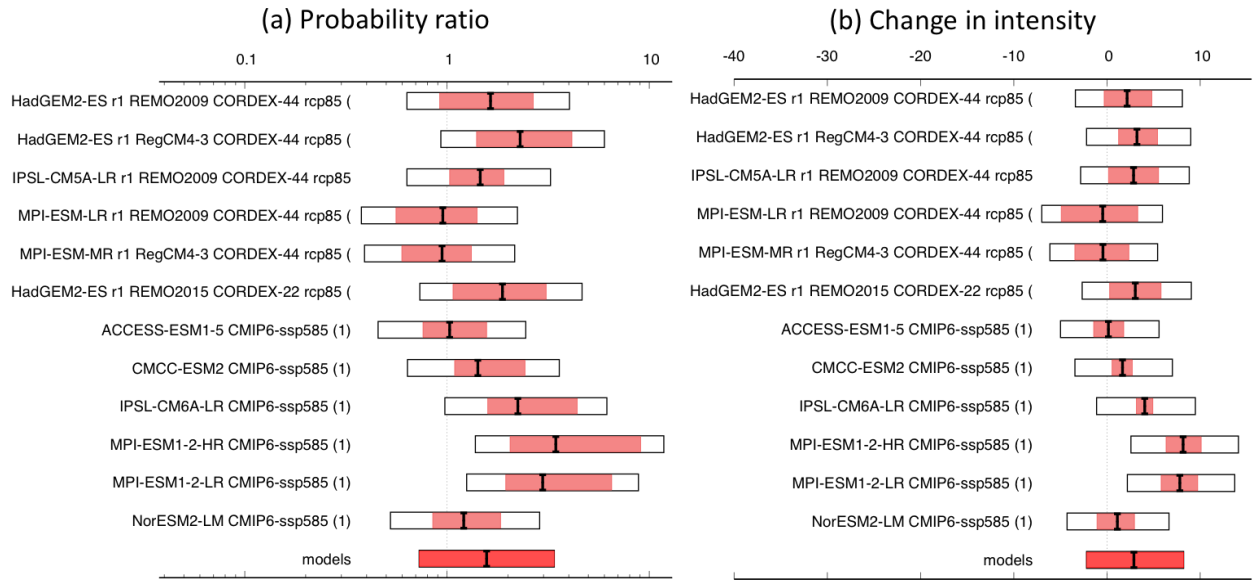


Fig. 6 As Fig. 5, but for models only of a 0.8°C warmer (2°C since pre-industrial) climate.

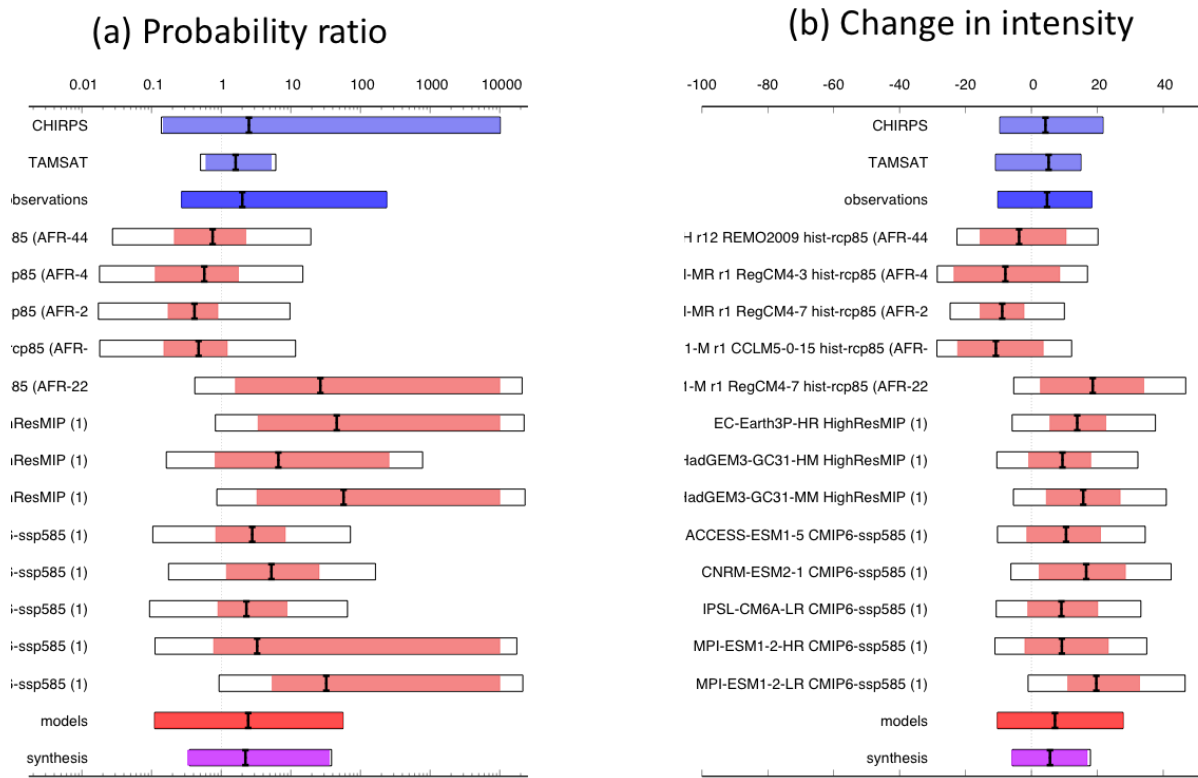


Fig. 7. Synthesis of (a) probability ratios and (b) intensity changes when comparing the return period and magnitudes of the maximum 7-day rainfall during 2022 JJAS season over Lower Niger, in the current climate and a 1.2°C cooler climate.

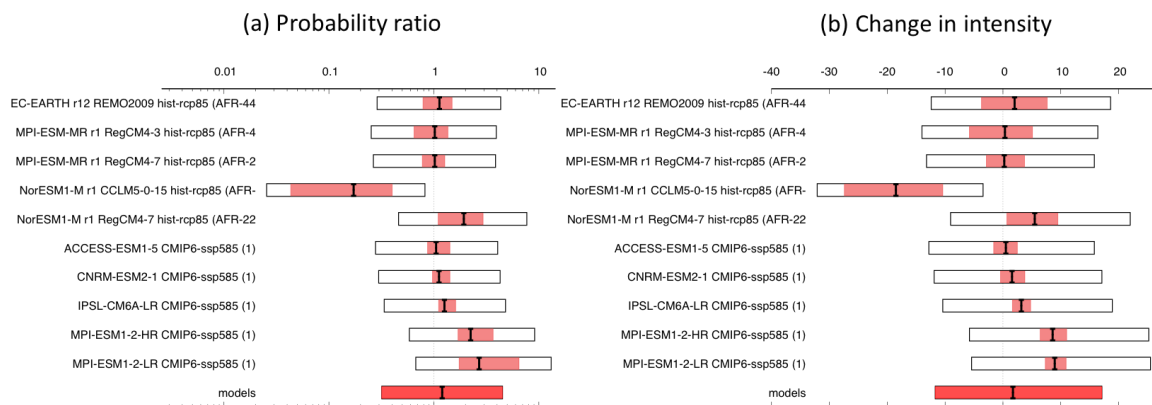


Fig. 8 As Fig. 7, but for models only of a 0.8°C warmer (2°C since pre-industrial) climate.

7 Vulnerability and exposure

In parts of West Africa in 2022, the rains arrived early and were more abundant than usual ([Ramadane, 2022](#)), leading to both fluvial and pluvial floods from Senegal to Cameroon ([UNHCR, 2022](#)). Nigeria and Niger saw the earliest onset of large floods in the first half of June, followed by Chad in July, Cameroon in August, and finally, Benin in September ([Sahara Reporters, 2022](#); [Africa News, 2022](#); [Reliefweb, 2022a](#); [Reliefweb, 2022b](#); [Davies, 2022](#)). In addition to the above-average rainfall, water releases from both Lagdo and Tiga dams over August and September were also reported to have contributed to an influx of water ([Mom, 2022](#); [Shuaibu, 2022](#)).

With at least 612 and 195 fatalities, respectively, the floods over Nigeria and Niger are among the deadliest in the countries' history ([Africa News, 2022](#); [Ruth, 2022](#)). The devastation in Nigeria is worse than the 2012 flood disaster with 34 out of 36 states and over 3.2 million people affected, including 1.5 million displaced and 2.776 injured ([Telesur English, 2022](#); [The Conversation, 2022](#); [Punch, 2022](#); [Addeh, Ajimotokan and Uzoho, 2022](#)). Several hundreds of thousands of hectares of land have been inundated, causing damage to more than 305.407 homes and 569.251 hectares of farmland ([Telesur English, 2022](#); [Asadu, 2022](#)). With at least 108 fatalities, the Minister of Humanitarian Affairs, Disaster Management, and Social Development has identified the state of Jigawa as worst affected following several flash floods over the rainy season ([Channels TV, 2022](#); [Maishanu, 2022](#)). Chad declared a State of Emergency on 19 October ([France24, 2022](#)). Out of the country's over 1.1 million affected people, nearly half (442.000) are displaced, and 22 deaths have been reported, across 18 out of the 23 provinces ([FRI, 2022](#); [CARE, 2022](#); [Reuters, 2022](#); [OCHA, 2022](#)). At least 56.607 homes, 465.000 hectares of crops, and numerous roads and bridges have been destroyed, with 1.112 water points and wells disrupted ([IFRC, 2022](#); [ECHO Daily Flash, 2022b](#); [CARE, 2022](#)).

The lingering floodwaters, coupled with disrupted water, sanitation and hygiene (WASH) services, are causing new and aggravating existing disease outbreaks in the affected countries. From January through September, cholera took 256 lives in Nigeria ([Outbreak News Today, 2022](#)). Since September, the water-borne disease has spread and is now plaguing the borderlands around Nigeria, Niger, Chad, and Cameroon, and has led to another 17 deaths ([Kindzeka, 2022](#); [Reliefweb, 2022c](#)). Vector-borne diseases such as malaria and yellow fever have also increased following the onset of the West African

rainy season ([WHO, 2022](#); [OCHA, 2022](#)). The floods, combined with damage to crops and assets, and increasing inflation (over 20% in August 2022) are acting as additional stressors to everyday people's lives.

7.1 Underlying vulnerability

In the 2021 Human Development Index, Nigeria, Niger, and Chad rank towards the bottom at 163, 189 and 190, respectively ([UNDP, 2022](#)). Driven by factors such as rapid population growth, precarious livelihood, high exposure to weather and climate shocks, and recently the COVID-19 pandemic, widespread poverty affects between 40 and 50 percent of the populations the three countries ([World Bank, 2018a](#); [World Bank, 2018b](#); [World Bank, 2018c](#); [OXFAM, n.d.](#)).

Income disparity in the region has reached extreme levels, as the richest one percent owns more than the remaining West African population combined ([Hallum and Obeng, 2019](#)). Gender disparities are also present, and decrease girls' school attendance and overall educational attainment, and increase the rates of child marriages, leading to low literacy and employment rates, ultimately disempowering girls and women to perceive the risks of and cope with floods ([Bang, Miles and Gordon, 2019](#)).

Inequality also extends to rural-urban dynamics. This is reflected in rural communities' lower access to public services such as healthcare and education, and higher rates of poverty and inequality, despite the rural economy's vital role in most West African economies ([Hallum and Obeng, 2019](#)). Notably, the agricultural sector employs 73, 35 and 75 percent of the populations across Niger, Nigeria and Chad ([World Bank, 2019a](#); [World Bank, 2019b](#); [World Bank, 2019c](#)), respectively, and accounts for 36.37, 29.94 and 53.99 percent of GDP, respectively ([Statista, 2021a](#); [Statista, 2022](#); [Statista, 2021b](#)).

Among West African governments' commitment to reduce inequality, Nigeria and Niger are ranked in the bottom three, along with Sierra Leone ([Hallum and Obeng, 2019](#)). Limited investments in tackling inequality - assessed by government spending on health, education and social protection, progressivity of tax policy, and labor rights and minimum wages - maintain structural vulnerabilities that are increasing peoples' susceptibility to extreme weather, such as the 2022 floods, ultimately making West Africa a vulnerability hotspot ([Fiorillo et al., 2018](#)). As highlighted by a recent WWA study (Brouillet et al., 2022), it is this chronic vulnerability that is driving the concurrent food crisis in Central Sahel, which is further aggravated by the floods as households lose limited food supplies and grain storages are destroyed ([ECHO Daily Flash, 2022](#); [Madjiangar, 2022](#); [Nkwunonwo, Whitworth and Baily, 2016](#)).

7.2 Urban development and informality

Since 2006, the majority of the global population has been residing in urban settings ([World Bank, 2018](#)). Africa is the the fastest urbanising region in the world with 40 percent of the population currently living in urban contexts, and by 2050, the percentage is projected to increase to 64 percent ([Anderson, Quinchia and Curiel, 2022](#); [Aliyu and Amadu, 2017](#); [Urban Africa, 2022](#)).

A majority of urban growth has been in small towns and secondary cities where more than half of the urban population resides in Africa ([Cities Alliance, 2022](#)). Despite this, secondary cities are often

under-resourced compared to their larger counterparts, undermining sustainable development ([Roberts and Hohmann, 2014](#)). Amongst other factors, a lack of finance drives challenges such as poor urban planning and governance, risky infrastructure, and an inability for populations to meet their basic needs ([Rouhana and Bruce, 2016](#); [Aliyu and Amadu, 2017](#); [Cities Alliance, 2022](#)). Some of the most serious consequences include accelerating rates of new developments on floodplains, and inadequate (in some cases non-existent) drainage and waste infrastructure ([Tazen et al., 2018](#); [Adeleye et al., 2019](#); [Nkwunonwo, Whitworth and Baily, 2016](#); [Bang, Miles and Gordon, 2019](#)). As more people migrate to urban areas, informal settlements are growing, and many of them are located in areas that are prone to landslides, floods, sea-level rise and storm surges which exacerbate existing vulnerabilities ([IPCC](#)). Notably, in the Niger River basin, settlements were constructed on levees and coastal plains during the drought period in the 1980s, leading to an increase of people in flood-prone areas when rainfall increased in recent decades ([Ogunkoya and Olayiwola, 2022](#)). In Nigeria, informal settlements house half of the urban population and are often located in flood-prone areas ([Ali, Akoteyon and Soladoye, 2021](#)).

Nigeria's urban population has surged from 10.1 to 58.3 percent between 1950 and 2020, and is projected to double over the next two decades ([Aliyu and Amadu, 2017](#)). This makes Nigeria one of the three countries which are expected to account for 37 percent of the world's urbanization over the coming 30 years ([Aliyu and Amadu, 2017](#)). Beyond the rapid natural population growth rate of 3.9 percent, Nigeria's urbanization is moreover driven by rural-urban migration, the development of the country's local government area (LGA) systems, the expansion of urban neighborhoods by annexation, and the evolution of rural villages to small urban communities ([Soulé et al., 2020](#); [Aliyu and Amadu, 2017](#)). The latter is a key cause to clearing of vegetation in peri-urban settings, increasing their exposure to flooding ([Umar and Gray, 2022](#); [Soulé et al., 2020](#); [Elagib et al., 2021](#); [Fiorillo et al., 2018](#)).

7.3 Water management

Twenty-eight transboundary river basins have been identified within the Economic Community of West African States (ECOWAS) region ([Niasse and Bossard, 2006](#)), with the most important ones being the Niger River Basin, shared between nine countries, the Senegal River Basin shared by four countries, the Volta River Basin, shared by six countries or the Lake Chad Basin (Lake Chad Basin Commission-LCBC) shared by six countries. Each of the West African countries shares at least one river basin with one of its neighbors, and in total the transboundary basins cover 71% of the total surface area of the region ([Niasse and Bossard, 2006](#)). Upstream water resource management of main water courses and their tributaries affects downstream water-related hazards. Transboundary basin authorities, such as the Niger Basin Authority (NBA), have been established in the region, in addition to the management of the different water uses, to reduce flood impact and vulnerability in their respective areas. However, information on transboundary floods in the region remains quite scarce.

The Lake Chad Basin borders seven countries, with a semi-arid climate and contributes water to Lake Chad. Naturally, transboundary water management issues arise, as the water is diverted for irrigation, hydropower generation and ecosystem services.

The Niger river meets its major tributary, the Benue in Nigeria. The Lagdo dam in Cameroon was constructed between 1977 and 1982 on the Benue river to generate hydroelectric power and facilitate the irrigation of crops downstream ([Tchotsoua et al., 2018](#)). This was during an era of increased dam construction in the region, and coincided with a historical 30 year drought in the Sahel (1968-1998) ([Ogunkoya and Olayiwola, 2022](#)). As rainfall recovered to pre-drought levels, the dams contributed to quasi-annual flooding in the Niger Delta linked to uncontrolled spillage of flood waters ([Ogunkoya and Olayiwola, 2022](#)).

During the current floods, many news reports pointed to an unexpected release of water from the Lagdo dam as a potential contributor to the floods ([The Cable, 2022](#); [The Nation, 2022](#)). However, water is released from Lago dam almost every year, so while its release may have contributed to the floods, without further study it is difficult to assess whether releases from the dam significantly contributed towards the exceptional human toll of the 2022 floods. A study of three other hydro-electric power dams upstream of the Niger delta found that they could not be the major cause of flooding given their limited contribution to water discharge during the relevant time period, but noted that the dams also could not be used to mitigate floods because they need to be as full as possible in order to maximize water pressure for electricity generation ([Ogunkoya and Olayiwola, 2022](#)).

In this case, risks cross country boundaries underscore the need for transboundary cooperation, and formal transboundary arrangements that can mitigate risks and generate cross-border benefits ([IPCC](#)). Improved transboundary governance is critical to accessing multilateral climate funds for transboundary investments. For example, the African Development Bank has supported countries in the Niger river to access climate funds for transboundary climate investments from the GCF and Global Environment Facility that could enhance resilient infrastructure and generate greater water benefits ([IPCC](#)).

7.4 Conflict, insecurity, and displacement

The region around Lake Chad and Lower Niger basins is highly exposed to the effects of climate change, but national and local factors mean that regions will experience cascading impacts. In both regions, conflict is mainly natural resources-based, and exacerbated by armed groups ([Vivekananda, Schilling and Smith, 2014](#)). Armed insurgencies in northeastern Nigeria, eastern Niger and parts of Cameroon and Chad have heightened insecurity in the region, and weakened state presence in some of the areas worst affected by the floods ([Brechenmacher, 2019](#)). Interacting with social, economic and political factors, these could exacerbate existing vulnerabilities and compound to increase the risk of violent conflict and forced displacement, even though the empirical evidence remains scarce ([SIPRI, 2021](#); [Millock & Withagen, 2022](#)). The political context is fragile in this region with Chad and Niger having experienced periods of military rule and, in parts, politics shaped by oil exploration ([adelphi, 2018](#)).

In Chad and Niger, as in most of the West Africa region, migration is an important adaptation strategy, but it can lead to conflict between host and migrant communities ([van der Geest et al., 2018](#); [Madgwick et al., 2017](#); [van der Land et al., 2018](#)). Some armed groups, predominantly Boko Haram, recruit from communities whose livelihoods are affected by factors including extreme weather; and local militias can escalate farmer–herder conflicts, thus eroding community resilience and increasing vulnerability. Already, conflict perpetrated by Boko Haram in the Lake Chad region has impacted 17.4

million people and has blocked access to waters that support farming and fishing, leaving people more vulnerable ([Akinyemi & Olaniyan, 2017](#); [Vivekananda, 2018, 2019](#); [Riebe and Dressel, 2021](#)). In Niger, conflict events have restricted livelihood activities and restricted freedom of movement with vast areas now militarized and declared no-go zones for civilians further compounding food insecurity and pushing people to adopt new, riskier coping strategies ([adelphi, 2018](#)).

Chad and Niger are also among the countries with the highest number of internally displaced people (IDPs) and refugees worldwide with 376,809 IDPs in Niger and 381,289 IDPs in Chad ([UNHCR, 2022](#)). The Internal Displacement Monitoring Centre (IDMC) records aggregated estimates on internal displacement due to conflict and weather-related events. In Niger and Chad, approximately 615,741 people live in displacement conditions as a result of conflict events and an additional 64,459 as a result of climate and weather-related events ([IDMC, 2022](#)). Between 2008 and 2021, 19 reported flood events have displaced over 1.9 million people in Niger ([IDMC, 2022b](#)) and 34 reported flood events displaced over 800,000 people in Chad ([IDMC, 2022c](#)). Flooding in the Lake Chad region displaced about 100,000 people along the active conflict zone of the Cameroon–Chad border in October 2019 ([European Commission, 2019](#)). Between 08 September and 29 October 2022, IDMC recorded flood-related 98,785 displacements in Chad and 4,961 displacements in Niger between 01 June and 04 September 2022, using destroyed houses as proxy for displacement ([IDMC, 2022b, 2022c](#)). During this time, violent conflict events and fear of attacks from non-state armed groups (NSAGs) added to the vulnerability layers, displacing around 16,000 people in Niger at the end of August 2022 at the border of Nigeria ([OCHA, 2022](#)).

7.5 Disaster risk reduction policy and adaptation

Over the last two decades, at least one-fifth of the Nigerian population - 42 million people - was impacted by flood disasters ([Salami, von Meding and Giggling, 2017](#)). The country has seen large-scale flooding at numerous occasions under the same time period, which is the most common and impactful hazard in Nigeria ([ECA, 2015](#)). Since 2010, analysis shows an increase in flood impacts, attributed to factors such as widespread poverty and rapid population growth which has led to an overall decline in resilience and coping capacity ([Fiorillo et al., 2018](#)). In 2012, Nigeria saw a disaster of similar extent, when 381 people died, over 7 million were affected of which 2.1 million people were displaced, and more than one million homes were damaged or destroyed ([ECA, 2015](#)). The floods cost the economy approximately US\$16.9 billion, which is equal to 1.4 percent of Nigeria's GDP ([Sidi, n.d.](#)).

Led by the National Emergency Management Agency (NEMA), Nigeria's mainstreaming of disaster risk reduction (DRR) into its policies and operations began in 2009 ([ECA, 2015](#)). The introduction of DRR has notably led to the development of an early warning system for floods, and today, disaster preparedness and response activities span several sectors ([Federal Ministry of Environment, n.d.](#); [Mashi, Oghenejabor and Ibrahim, 2019](#)). Still, shortcoming in the response to the 2012 floods demonstrated that the government had a long way to go to realize its potential, with community involvement pinpointed as a distinct weakness ([Buba et al., 2021](#)). By 2015, due to a lack of funding, only 22 out of 36 states had set up their respective emergency management agencies and roughly three-fourths were operating with little capacity, while no local government councils had established committees for emergency management ([ECA, 2015](#)). To date, despite NEMA's repeated calls for it, only a few states have set up emergency management committees ([Vanguard, 2022](#)).

The early and abundant rainfall in 2022 was well anticipated by the Regional Climate Outlook Forum for West Africa, which disseminated an alert in May ([Centre Régional AGRHYMET, 2022](#)). While Nigeria is still in the process of developing an early action protocol (EAP), and with that an anticipatory humanitarian action mechanism for flooding, the Nigerian Red Cross Society (NRCS) was granted imminent DREF funding to undertake early action ([IFRC, 2022](#)). Similarly, the EAP in Niger was triggered, releasing predetermined financing to enable the Red Cross Society of Niger (RCSN) to roll out early actions such as prepositioning of household items including water containers and mosquito nets, setting up emergency shelters, evacuation of at-risk populations, and sensitization activities ([Anticipation Hub, 2022](#)). Following the devastation, extensive response operations have moreover been mobilized in collaboration with NEMA by the International Organization for Migration (IOM), the Food and Agriculture Organization (FAO), the World Food Programme (WFP), Save the Children, the UN Children’s Fund (UNICEF), the World Health Organization (WHO), the UN High Commissioner for Refugees (UNHCR), and Action Against Hunger (AAH) ([OCHA, 2022](#)).

In addition to managing the immediate impacts of the floods, long-term policies such as housing and infrastructure zoning can be another tool for reducing the exposure of infrastructure and people to flood prone areas, but it requires good governance and enforcement to be effective.

Data availability

Almost all data are or will soon be available via the Climate Explorer.

References

All references are hyperlinked in the main text.